THE ADVANCED X-RAY IMAGING SATELLITE

Authors: Richard F. Mushotzky[1], James Aird[2], Amy J. Barger[3], Nico Cappelluti[4], George Chartas[5], Lía Corrales[6], Rafael Eufrasio[7,8], Andrew C. Fabian[9], Abraham D. Falcone[10], Elena Gallo[6], Roberto Gilli[11], Catherine E. Grant[12], Martin Hardcastle[13], Edmund Hodges-Kluck[1,8], Erin Kara[1,8,12], Michael Koss[14], Hui Li[15], Carey M. Lisse[16], Michael Loewenstein[1,8], Maxim Markevitch[8], Eileen T. Meyer[17], Eric D. Miller[12], John Mulchaey[18], Robert Petre[8], Andrew J. Ptak[8], Christopher S. Reynolds[9], Helen R. Russell[9], Samar Safi-Harb[19], Randall K. Smith[20], Bradford Snios[20], Francesco Tombesi[1,9,21,22], Lynne Valencic[8,23], Stephen A. Walker[8], Brian J. Williams[8], Lisa M. Winter[15,24], Hiroya Yamaguchi[25], William W. Zhang[8]

Contributors: Jon Arenberg[26], Niel Brandt[10], David N. Burrows[10], Markos Georganopoulos[17], Jon M. Miller[6], Colin A. Norman[17], Piero Rosati[27]

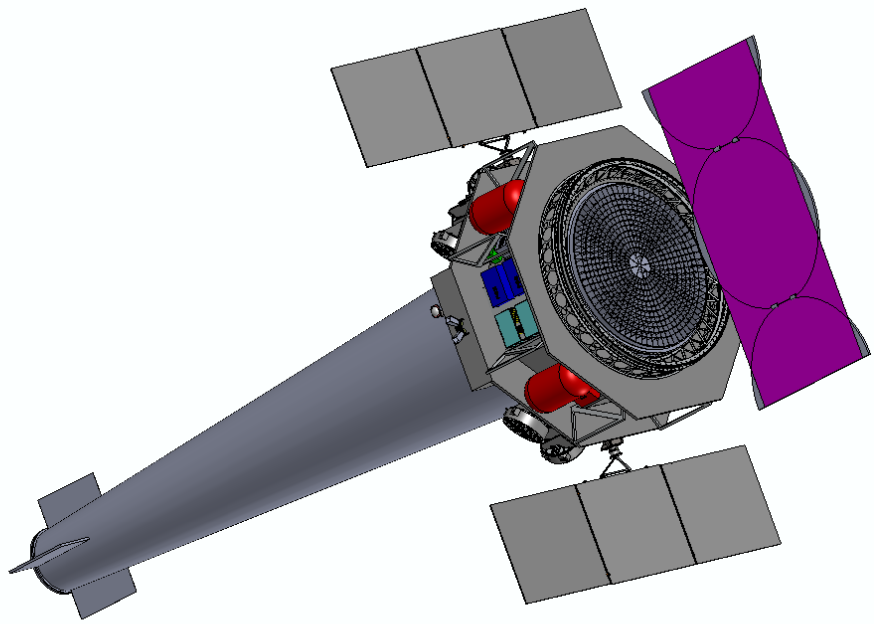

A Probe-class mission study commissioned by NASA for the NAS Astro2020 Decadal Survey

July 10, 2019

AUTHOR AFFILIATIONS

[1] Department of Astronomy, University of Maryland, College Park, MD 20742

[2] Department of Physics and Astronomy, The University of Leicester, Leicester LE1 7RH, UK

[3] Department of Astronomy, University of Wisconsin-Madison, Madison, WI 53706

[4] Physics Department, University of Miami, Coral Gables, FL 33124

[5] Department of Physics and Astronomy, College of Charleston, Charleston, SC 29424

[6] Department of Astronomy, University of Michigan, Ann Arbor, MI 48109

[7] The Catholic University of America, Washington, DC 2006

[8] NASA Goddard Space Flight Center, Greenbelt, MD 20771

[9] Institute of Astronomy, Cambridge CB3 0HA, UK

[10] Department of Astronomy and Astrophysics, Pennsylvania State University, University Park, PA 16802

[11] INAF-Osservatorio Astronomico di Bologna, 40129, Bologna, Italy

[12] Kavli Institute for Astrophysics and Space Research, Massachusetts Institute of Technology, Cambridge, MA 02139

[13] Centre for Astrophysics Research, University of Hertfordshire, Hatfield, Hertfordshire, QQ62+JJ, UK

[14] Eureka Scientific, Oakland, CA 94602

[15] Center for Theoretical Astrophysics, Los Alamos National Laboratory, Los Alamos, NM 87545

[16] Johns Hopkins University Applied Physics Laboratory, Laurel, MD 20723

[17] Department of Physics, University of Maryland Baltimore County, Baltimore, MD 21250

[18] Carnegie Observatories, Pasadena, CA 91101

[19] Department of Physics and Astronomy, University of Manitoba, Winnipeg, MB R3T 2N2, Canada

[20] Harvard-Smithsonian Center for Astrophysics, Cambridge, MA 02138

[21] Department of Physics, University of Rome Tor Vergata, 00133, Rome, Italy

[22] INAF Astronomical Observatory of Rome, 00078, Monteporzio Catone, Italy

[23] Department of Physics & Astronomy, Johns Hopkins University, Baltimore, MD 21218

[24] National Science Foundation, Alexandria, VA 22314

[25] Institute of Space and Astronautical Science, Sagamihara, Kanagawa 252-5210, Japan

[26] Northrop Grumman Aerospace Systems, Redondo Beach, CA 90278

[27] Department of Physics and Earth Science, University of Ferrara, 44122, Ferrara, Italy

1 SUMMARY

The evolution of astronomy from isolated disciplines centered on specific wavelengths to panchromatic and multi-messenger science is the legacy of the last 50 years of research. X-ray observations are a crucial part of this, and key advances in optics and detector technology have paved the way for a mission that surpasses *Chandra* in angular resolution by a factor of ∼2 and sensitivity by an order of magnitude. This mission will transform the following areas of astrophysics:

- The growth and fueling of supermassive black holes
- The transient universe
- Galaxy formation and evolution
- The microphysics of cosmic plasmas
- A wide variety of cutting-edge observatory science

The *Advanced X-ray Imaging Satellite (AXIS)* will make these scientific advances within the constraints of a Probe-class mission. This is due to imaging capabilities (see Table 1) that exceed both *Chandra* and ESA's planned *Athena* mission (see Figure 1). **This document is a summary of the full 50-page *AXIS* study report submitted to NASA, available at arXiv:1903.04083.**[1]

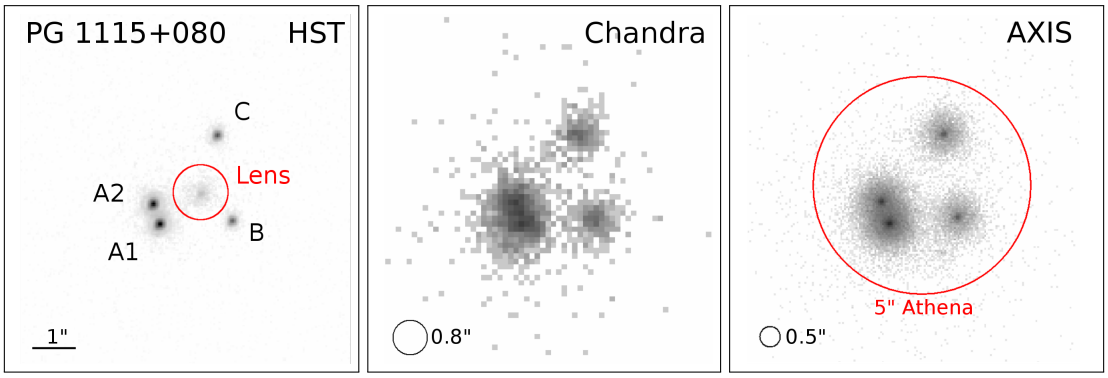

Fig. 1 — *AXIS* can measure the innermost stable circular orbit and spin of the supermassive black hole in a quadruply-lensed quasar (*HST* image at left) through monitoring variability of the quasar's multiple lensed images (A1, A2, B, C). The 30 ks *Chandra* image (0.8″ HPD) has limited photon statistics and does not separate A1 and A2, whereas a 30 ks *AXIS* exposure (0.4″ HPD) will yield high-quality spectra from each quasar image and variability on timescales much shorter than those accessible by *Chandra*. The 5″ *Athena* PSF is shown in the right panel.

AXIS has a rapid spacecraft response and straightforward mission operations, giving high observing efficiency and permitting extensive time domain science at 100 times the sensitivity of the Swift XRT. This opens up a vast discovery space, and complements the next generation of astronomical observatories (such as *JWST*, *WFIRST*, LSST, SKA, TMT, ELT, CTA), while providing an extensive guest observer (GO) program. The strong synergy between *Chandra* and *XMM-Newton* shows that having a complementary high-throughput, high-spectral resolution spectroscopic mission (*Athena*) operating at the same time as *AXIS* greatly increases the range of science discovery.

The simplicity of *AXIS* — a single mirror and detector, and few moving parts — results in a robust, low cost design. *AXIS* builds on developments in X-ray mirror technology over the past decade that will produce high-angular resolution lightweight X-ray optics at reasonable cost, utilizing precision polishing and thin single-crystal silicon mirrors. An angular resolution better than 1″ after accounting for gravity distortion for a mirror pair module was demonstrated in 2019, and recently, mirror segments with 0.5″ performance have been regularly fabricated at GSFC. The *AXIS* spacecraft design was developed during NASA/GSFC Instrument (IDL) and Mission (MDL) Design Lab studies, and uses proven components and methods to meet requirements. The estimated mission cost is consistent with the $1B Probe mission cost cap in 2018 dollars.

Parameter		Value	*AXIS* vs. *Chandra*
Angular resolution	on-axis	$0.4''$	$2\times$ sharper
(HPD, at 1 keV)	$15'$ off-axis	$1''$	$28\times$ sharper
Energy band		0.2-12 keV	Similar
Effective area	at 0.5 keV	7000 cm^2	$15\times$ more collecting area
(mirror + detector)	at 6.0 keV	1500 cm^2	$6\times$ more collecting area
Energy Resolution	at 1.0 (6.0) keV	60 (150) eV	Similar
Timing Resolution		< 50 ms	$6\times$ brighter pile-up limit
Field of View (FoV)	HPD $\lesssim 1''$	$24' \times 24'$	$70\times$ better for $< 1''$ imaging
Detector Background	at 1 keV	2×10^{-4} ct/s/keV/arcmin^2	$50\times$ better sky/background
Slew Rate		120° / 5 min	Comparable to *Swift*

Table 1 — *AXIS* mission parameters compared with *Chandra* best-in-class values (at launch).

2 KEY SCIENCE OBJECTIVES

AXIS complements the portfolio of the next decade, including *WFIRST*, LIGO, 30m-class telescopes, and the high X-ray spectral resolution *Athena* mission. It will enable breakthroughs in many issues raised by the Astro2020 Science White Papers (Table 3) via community participation in an extensive guest observer program. A few key science topics are detailed below.

2.1 The Growth and Fueling of Supermassive Black Holes (SMBHs)

X-rays are the cleanest, most unbiased wavelength to identify and quantify SMBH growth and fueling, and can probe the regions very close to the black hole, even for quasars at $z = 2$.

The existence of $\sim 10^9 M_\odot$ black holes only 800 Myr after the Big Bang is a major unsolved problem, requiring either extremely rapid growth from Pop III remnants in the early universe or the direct collapse of $10^{4-6} M_\odot$ seeds of gas. *AXIS* will address the early growth of black holes through deep and wide angle surveys, which will detect $\sim$100 SMBHs at z>6, the progenitors of the newly discovered $z \sim 7.5$ quasars out to z =13, and $>10^5$ AGN across all redshifts. The deep and wide surveys will require $\sim$ 10% of the *AXIS* observing time over a 5-year period, and will measure the redshift-dependent luminosity function to $z > 8$[4].

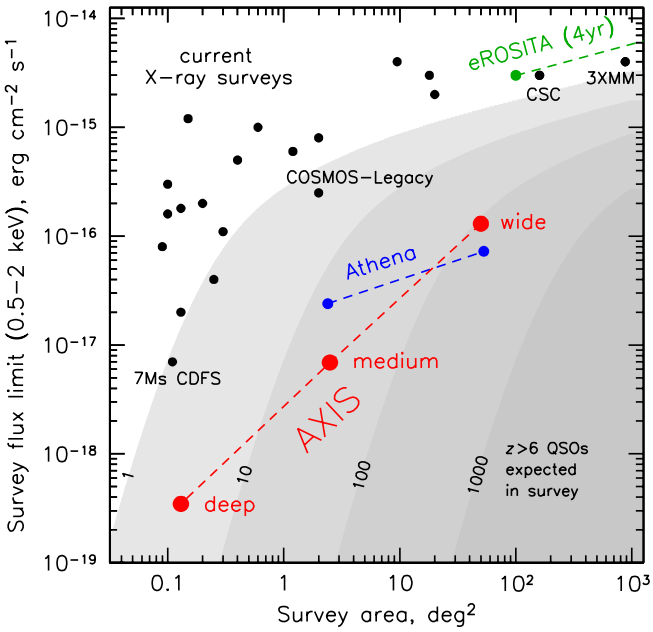

Fig. 2 — Area vs. flux limit for planned *AXIS* surveys compared with *Chandra*, *XMM*, *Athena* (1-year) and *eROSITA* surveys. Grayscale shows the number of expected $z > 6$ AGN detectable in the survey[2,3], black dots present day surveys.

Figure 2 illustrates how *AXIS* will exceed current and future surveys. While *Athena* will detect a similar number of bright high-z AGN, sub-arcsecond resolution is needed to identify their hosts and disentangle high-z AGN progenitors from star forming galaxies[5,6]. Meanwhile, most high-z AGN will be obscured, making it difficult for *WFIRST* or LSST to isolate their signal.

The unique identification of counterparts and the wide range of multi-wavelength data will determine the correlation of the AGN nuclear properties as a function of mass and star formation rate. In addition, these surveys will greatly expand the sample of "dual SMBHs" out to $z \sim 2$, as X-rays are the most efficient and robust way to detect them[7]. These results will measure the rate of binary BH formation, the population from which *LISA* sources are drawn[8].

AXIS will provide an unprecedented view of the process of accretion by imaging the Bondi radius for at least 25 nearby non-AGN SMBHs, compared to the two that *Chandra* has imaged[9,10,11]; Figure 3). Those observations imply the presence of both rapidly cooling inflows and strong outflows. *AXIS* will measure the temperature and density of the gas and strongly constrain theories of BH accretion, determining why most BHs in the local universe are not radiating. Beyond expanding the sample, we will perform spatially resolved spectroscopy that is not possible with *Chandra*.

AXIS can probe even closer to the SMBH, on the scale of the Event Horizon Telescope, when aided by gravitational lenses. Microlensing (by stars) of quasars behind galaxies produces caustics that magnify as they sweep over the quasar[12,13]. The detection of individual caustic crossing events will be spectacular, revealing the gradual change in continuum and the profile and energy of the 6.4 keV Fe Kα line as the caustic sweeps over the accretion disk and corona, directly measuring their origin. Comparing the X-ray and optical variability constrains the structure of the accretion disk[14], the size of the hot corona, inner accretion flow, and dusty torus, and the spin of the black hole[15]. Already, *Chandra* observations of a handful of quasars show that the X-ray emitting corona is very compact[16,17],with one source having a well determined spin and size[18], but this sample cannot be expanded. *LSST* will provide a pool of >4,000 lensed quasars with $0.5 < z < 5$ for *AXIS* to follow up and study their evolution, providing notice of caustic crossings.

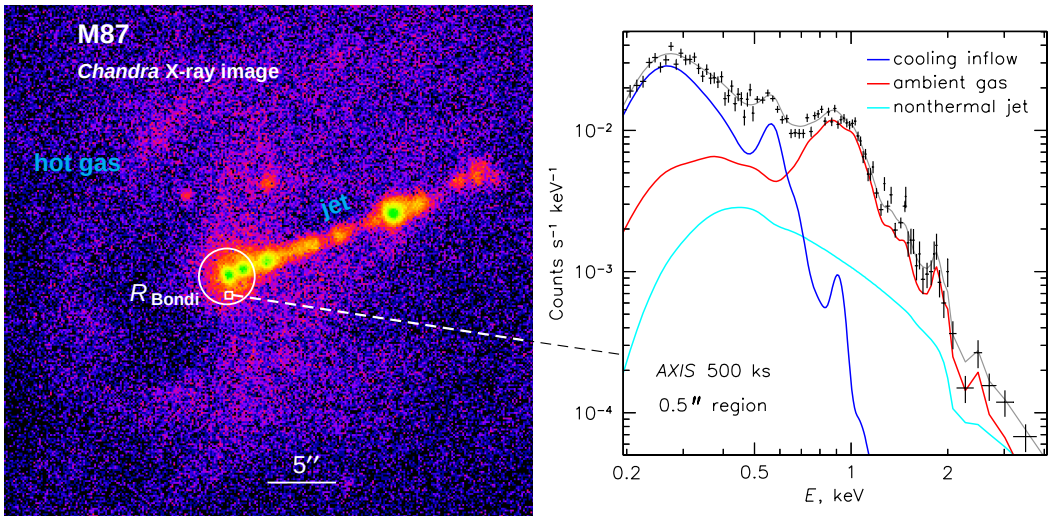

Fig. 3 — *Left*: *AXIS* will map the accreting gas that fuels SMBH in detail. The black hole's sphere of influence is shown by the white circle on this *Chandra* image of M87. *Chandra*'s resolution and soft X-ray response limit studies of the gas properties within this region. *Right*: A simulated *AXIS* spectrum for a $0.5'' \times 0.5''$ region (box in left panel) from a 500 ks observation. *AXIS* will map the rapidly cooling, inflowing gas with $kT < 0.5$ keV (blue curve).

2.2 The Transient Universe

X-ray follow-up observations are an efficient tool for identifying transients because (1) they can quickly localize transients with large positional errors, and (2) X-rays can reveal the nature of transients that may not have unique signatures at other wavelengths.

The 2010 Decadal Survey ranked LSST as the highest priority project for ground-based astronomy, indicating that time-domain astronomy is an essential component in understanding our

universe. LSST, SKA, and LIGO will vastly increase the detection of transient sources. Many of these, from stellar flares and novae to binary neutron star mergers and tidal disruption events (TDEs) are X-ray emitters, and the keys to successful follow-up are high sensitivity and rapid, flexible response. *AXIS* has a rapid re-pointing response with operations similar to *Swift*, but is **100 times more sensitive than the Swift XRT for time domain science. Based on the desires of the GO community, AXIS could devote at least 10% of its observing time to studies of transient objects.**

TDEs, the capture and tidal disruption of a star,[19] are laboratories for super-Eddington flows[20] and accretion state transitions. X-rays probe the region closest to the SMBH, necessitating sensitive X-ray monitoring, currently done by *Swift*. *AXIS* will enable spectroscopic monitoring of much larger samples of more distant and intrinsically less luminous TDEs discovered by LSST. TDEs are a promising way to detect BHs too small to detect dynamically, and find new and unexpected phenomena like the recent off-nuclear X-ray TDE candidate with a BH mass of $10^{4.5-5} M_\odot$[21].

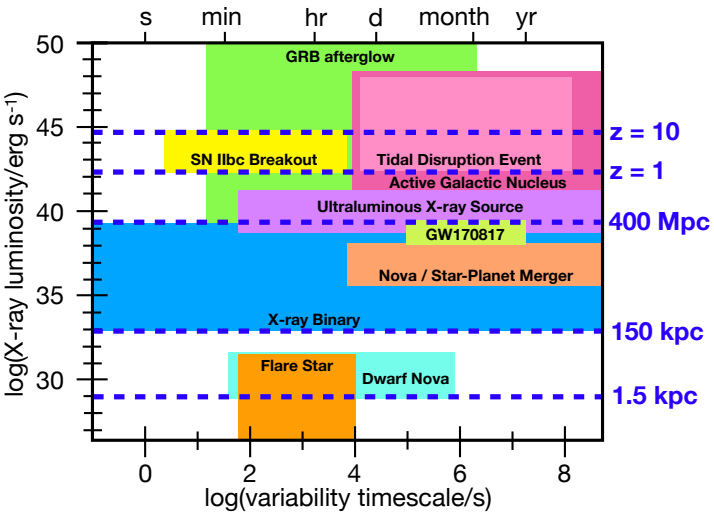

Fig. 4 — The X-ray luminosity and variability timescale of various astrophysical phenomena. AXIS is designed to follow-up transients from future all-sky monitors like LSST and LIGO that will probe much larger distances. The right axis (in blue) denotes the distance out to which AXIS can detect these transients in just 20 ks.

In the era of multi-messenger astronomy, X-ray afterglows from LIGO GW events will be vital in interpreting the multi-band spectra and light curves of these events. X-ray observations constrain the external density, magnetic field, jet structure[22], and binary inclination (breaking the degeneracy from GWs alone). In the 2020s, most GW events will be found at $d \sim 200-400$ Mpc. If these events are similar to GW170817, their X-ray afterglows will be too dim for *Chandra*. *AXIS* could detect such afterglows in short $5-20$ ks exposures, identifying and monitoring the source.

Arcsecond angular resolution is the key to such followups. At 200 Mpc, a similar event to GW170817 would be $2''$ away from the nucleus; *Athena*, with its $5''$ resolution, would not be able to distinguish the event from an AGN, ultraluminous X-ray source (ULX), or magnetar, since these sources are highly variable and of similar luminosity to a GW event, and could be confused with the neutron star merger.

With *LISA* scheduled to launch in the 2030s, it is important to understand how to obtain the electromagnetic counterparts to the LISA GW sources. The strongest candidates will be AGN-like sources in mergers; *AXIS* can detect an "average" $10^6\ M_\odot$ merger at $z = 2$ with 2-hr exposures, allowing a sensitive search of 1 sq degree LISA error boxes in less than a day[23].

AXIS will serendipitously detect transients, like ULXs, novae, and core-collapse SN, out to significant distances (Figure. 4). Within a distance of 250 Mpc, *AXIS* will detect an average of $\sim$1.5 MW-mass galaxies per field of view; in a 50 ks exposure, it will detect all of the ULXs in those galaxies. With a $<$50 ms time resolution, we can search for ULX pulsation[24]. *AXIS* can detect classical novae ($L_X \sim 10^{35}$ erg s^{-1}) out to a distance of $\sim$1 Mpc, allowing X-ray flux measurements for all classical novae in the Local Group. Core-collapse SNe have $L_X \sim 10^{38-41}$ erg s^{-1}. *AXIS* can detect a SN with $L_X \sim 10^{40}$ erg s^{-1}at a distance of 400 Mpc, allowing access to thousands of SNe per year.

2.3 Galaxy Formation and Evolution

X-ray emission can measure the metallicity, temperature and density of the hot gas around galaxies that serves as both their long-term source of fuel and the depository of feedback energy, mass, and metals.

AXIS will characterize the hot gas around and between galaxies and measure SNe and AGN feedback across cosmic time. It will trace star formation to $z > 3$ through the well-determined scaling relation between the X-ray luminosity and star formation rate[26,27]. At $z > 1$, many galaxies have SFR $\geq 100\ M_\odot\ \mathrm{yr}^{-1}$ and will be detected by *AXIS* in $100-300$ ks exposures. With its high resolution, *AXIS* can separate the AGN, X-ray binary emission, and circumgalactic medium (CGM), important as these systems frequently host obscured AGN. For lensed galaxies[28,29], *AXIS* can spatially resolve and characterize the hot ISM at $z > 3$.

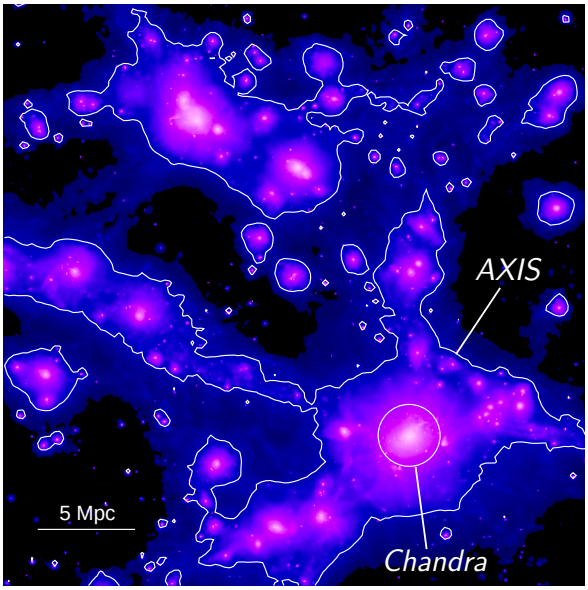

Fig. 5 — In this simulation of large scale structure[25], color shows X-ray brightness of the IGM, revealing a web of filaments with galaxy clusters as bright nodes and galaxies and groups along the filaments. *AXIS* will be able to reach much farther into those dynamic, but very dim regions (the white contour) than any other X-ray instrument.

AXIS will also detect the raw material for galaxy growth and the results of feedback which produce the hot circumgalactic and intergalactic medium (CGM/IGM). While ΛCDM models predict that $L*$ galaxies are surrounded by extended hot halos which contain the majority of the baryonic and metal content[30,31], direct detection of this hot gas is presently limited to a only a handful of massive spiral galaxies[32]. *AXIS* will detect and characterize the hot CGM around many individual L_* galaxies within $d < 200$ Mpc. Owing to its low background, *AXIS* will be able to study the gas in galaxy clusters out to twice the cluster virial radius (Figure 5), testing cosmic structure formation theories[33] at the interface between the clusters and the vast cosmic web.

High-resolution *Chandra* images of a few nearby clusters, such as Perseus, reveal rich AGN-induced structure[34], but the detailed processes which heat the intracluster medium are unclear. *AXIS* maps of density, temperature, and non-thermal emission on 0.5–10″ scales in combination with high resolution spectra from *Athena*, over a wide range of redshifts, masses, and cooling rates, can untangle the AGN heating mechanisms. The same processes should also operate in galaxy groups and individual galaxies[35], enabling a detailed study of feedback at all scales.

SMBHs play a central role in regulating the growth of massive galaxies. The energy released as they grow (and shine as an AGN) can heat up and/or expel star forming gas from the galaxy[36]. The physical processes underlying AGN feedback and how they scale are amongst the most pressing problems in galaxy evolution. *AXIS* can resolve the shock interaction between the ISM and AGN wind in > 20 nearby systems and search for non-nuclear AGN related emission. Combined with ALMA and *Athena* tomography, this will constrain radiative feedback models[36].

During periods of intense star formation, multiple SNe combine to drive multiphase galactic winds[37,38]. In survey fields, *AXIS* can detect strong winds (like that in NGC 6240; $L_X > 10^{41}$ erg s^{-1}) out to $z \sim 1$ and characterize large samples of starburst galaxies at lower redshift. *AXIS* can also probe how HMXBs contribute to reionizing the Universe at $z > 6$ by studying how they ionize and remove gas enshrouding young star clusters in low-z Lyman-break analogs[39,40,41].

2.4 The Microphysics of Cosmic Plasmas

X-ray observations can uniquely measure the fundamental physical parameters of hot plasmas, such as their viscosity, shock structure, thermal conductivity, magnetic fields, diffusion coefficients and equilibration timescales.

Plasma physics often forms the physical basis in models for many complex phenomena in the Universe, from solar flares to galaxy formation to the emergence of large scale structure. Precision cosmological tests based on galaxy clusters are only as precise as our understanding of the cluster plasma physics. Models of the growth of structure and black hole feedback rely on energy transport in hot, tenuous plasma, but the viscosity, heat conductivity, energy exchange between thermal particles, cosmic rays and magnetic fields, are poorly known. *AXIS* is uniquely suited to probe these properties through finding and studying shocks and other sharp features in many astrophysical plasmas, such as those in galaxy clusters and supernova remnants (SNRs).

Shock front structure, as observed in X-rays, can diagnose several plasma physics processes. For example, *Chandra* has attempted to constrain the electron-ion equilibration timescale in three clusters[42] by resolving the shock electron temperature profile, with contradictory results[43,44,45]. *AXIS* will perform this test, only possible in clusters, in many shocks. X-ray observations of the sharpness and structure of contact discontinuities ("cold fronts") in clusters[46] may diagnose the plasma viscosity and thermal conductivity. Cold fronts are produced by "sloshing" of gas in the cluster potential[47], which leads to velocity shear across the front and Kelvin-Helmholtz instabilities, unless they are suppressed by viscosity[48,49]. *Chandra* has discovered such instabilities in a few cold fronts and bounded the effective isotropic viscosity to $<1/10$ of the classical value[50,51,52,53]. By vastly increasing the accuracy and sample size, *AXIS* will determine if significant nonzero viscosity is required. Faint tails of stripped gas behind infalling galaxies is another sensitive viscosity diagnostics that *AXIS* will advance.

Fast (several thousand km s^{-1}) SNR shocks are characterized by thin rims of X-ray synchrotron emission, and probe magnetic field amplification. However, only a few synchrotron-dominated shocks can be studied with *Chandra*[54,55], and many examples are needed to understand field amplification. Faint X-ray emission ahead of the shock is also expected from cosmic-ray diffusion, but has yet to be detected[56]. Finding this precursor will constrain the diffusion and scattering lengths of cosmic rays — a strong complement to gamma-ray observations. In very dim outskirts of galaxy clusters, *AXIS* will be able to find numerous shock fronts that are sites of acceleration of ultrarelativistic cosmic rays. Studying them jointly with current and future low-frequency radio arrays such as LOFAR will greatly advance our understanding of particle acceleration in plasmas.

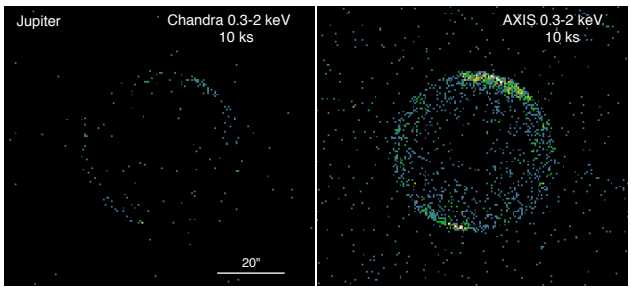

Fig. 6 — Simulated *Chandra* (left) and *AXIS* (right) observations of Jupiter's aurora. *AXIS*will resolve daily fluctuations in Jovian X-ray emissions and magnetic field reconnections on 1000-km scales, allowing a comparison of these changes to daily auroral and atmospheric weather events.

2.5 Observatory Science with AXIS

From understanding the habitability of exoplanets to mapping ISM dust in our galaxy, X-ray imaging provides a unique and complementary probe to a range of science topics.

Like *Chandra*, *AXIS* will be a general purpose astronomical observatory that is **primarily guest observer driven**. This document can describe only a fragment of the science that *AXIS* will advance. *AXIS* data will be crucial for studying supernovae and SNRs, magnetars and pul-

sar wind nebulae, timing of ULXs and X-ray binaries in the local group, galaxies and pulsars, stellar coronae and star-forming regions, dust properties in the MW and M31, the galactic center, and even solar system targets like comets, the Moon, and Jupiter (see Figure 6). The *AXIS* spatially resolved data will be complementary to the detailed studies of spectral lines with *XRISM* and *Athena*). The legacy, begun by *Chandra*, of high-spatial resolution imaging of the X-ray universe can be continued and dramatically enhanced within the scale of a Probe-Class mission.

3 TECHNICAL OVERVIEW

A full description of the *AXIS* mission implementation is given in our report to NASA HQ, available on arXiv[1]. Here, we give a *brief* summary of the technologies required for the mission.

3.1 AXIS Mirror Assembly

The design and implementation of the *AXIS* mirror assembly drives the *AXIS* science performance and programmatic requirements on mass, volume, production cost, and schedule. It incorporates knowledge and lessons learned from designing and building mirror assemblies for past and current observatories, including *Chandra*, *XMM-Newton*, *Suzaku*, and *NuSTAR*. The *AXIS* mirror assembly is made possible by the recent conception and development of the silicon meta-shell optics technology pursued by the Next Generation X-ray Optics (NGXO) team at NASA GSFC. The design, described below, results in a 9-m focal length mirror, with inner and outer diameters of 300 and 1700 mm, respectively. A total of 16,568 mirror segments (each 100mm $\times$ 100mm $\times$ 0.5mm) are arranged into 188 mirror modules, which are then grouped into 6 metashells. These 6 metashells are assembled into the final mirror assembly, which has a total mass of only 454 kg.

Silicon meta-shell optics technology, in development since 2012, combines the precision optical polishing technology that enabled *Chandra*'s exquisite PSF with the use of mono-crystalline silicon material, fabricated into 0.5mm thick mirrors[57]. The process takes advantage of the ready availability of mono-crystalline silicon, along with the equipment and processing knowledge accumulated by the semiconductor industry. This technology meets the three-fold requirement on the *AXIS* X-ray mirror assembly: (1) better PSF than the 0.5″ *Chandra* mirrors, (2) more than 10 times lighter per unit effective area, and (3) more than 10 times less expensive per unit effective area.

There are four major steps in building the *AXIS* mirror assembly, shown in Figure 7: (1) mirror segment fabrication, (2) integration of mirror segments into mirror modules, (3) integration of mirror modules into mirror meta-shells, and (4) integration of mirror meta-shells into the final mirror assembly. The *AXIS* mirror assembly is made of silicon, with only trace amounts of foreign materials. This effectively uniform composition enables the mirror assembly to operate at a temperature different from room temperature at which it is built and tested, significantly reducing logistical complexity and the costs of building, testing, and operating. The excellent thermal conductivity of silicon (two orders of magnitude higher than glass) enables AXIS to meet the stringent PSF requirements in a low-earth orbit environment. The mirror segment's production is highly

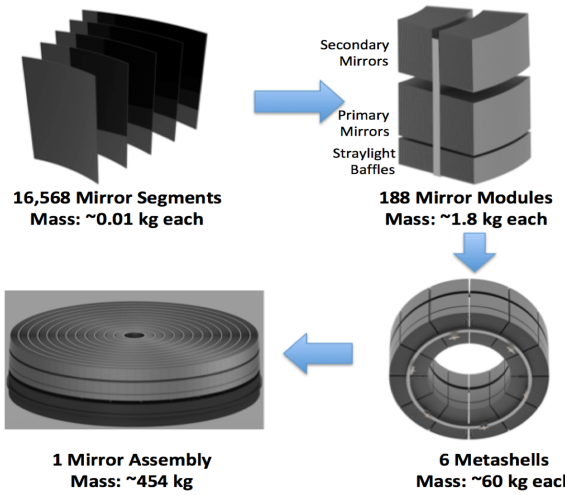

Fig. 7 — A hierarchical approach to build the AXIS mirror assembly that enables mass parallel production. It uses commercially available materials and equipment to minimize both production cost and schedule.

similar to the wafer production process, allowing use of commercially available equipment and knowledge to minimize cost and schedule, and the modular approach is highly amenable to parallel production. The large numbers of mirror modules and meta-shells make it easy to manage spares, and their modest size requires no special equipment to handle, test, or qualify.

3.2 AXIS Detector Assembly

The design of the *AXIS* focal plane is meant to take advantage of the *AXIS* PSF. The key technical challenges are small pixel size to sample the PSF, readout at high rate with sufficiently low noise to ensure good low energy response, and fast, low-noise on-board processing electronics. The *AXIS* design exploits ongoing technical advancements toward "fast, low-noise, megapixel X-ray imaging arrays with moderate spectral resolution," identified by the 2017 Physics of the Cosmos Program Annual Technology Report as a top-priority technology development*. Our plan utilizes both fast parallel-readout CCDs[58], capitalizing on decades of heritage provided by X-ray CCD detectors used to great success aboard *Chandra*, *Suzaku*, *Swift*, and *XMM-Newton*; and fast, low-power CMOS active pixel sensor with less heritage but showing very promising developments. The final design will likely incorporate a single detector technology, simplifying many aspects of the focal plane, reducing risk and cost.

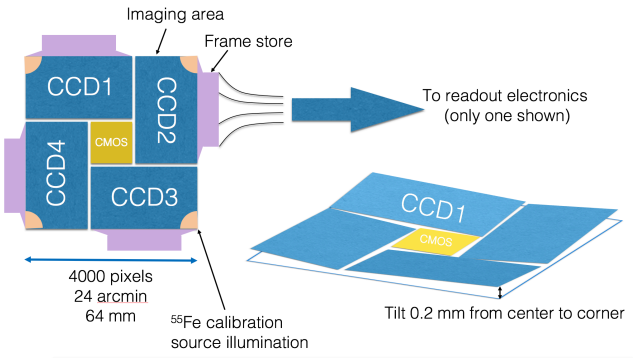

Fig. 8 — The baseline Focal Plane Array uses a CCD/CMOS hybrid design. Both technologies are included to capitalize on parallel technological development; the final design will likely use a single detector technology.

The *AXIS* Focal Plane Assembly (FPA) uses four 1.5k×2.5k CCDs to tile the majority of the focal plane, and a single, smaller 1k×1k CMOS in the center (see Figure 8) to minimize pile-up of bright targets. The CCDs are tilted to match the curved focal plane, minimizing image distortion. Both detector types are back-illuminated and fully depleted to 100 μm to ensure high quantum efficiency (QE) across the *AXIS* band of 0.2–12 keV. The 16μm (0.37″) pixel size is sufficient to sample the 0.4″ telescope HPD, because charge from a single photon is spread across multiple pixels and can be centroided through sub-pixel positioning[59,60] to better than 0.1″, significantly better than that of *Chandra's*. A readout noise of less than 4 e^- ensures good soft response[61].

Both types of detectors are baselined to read out at 20 frames/sec (fps) for normal observations — 64× that of *Chandra* ACIS — but the CMOS can read out faster than 100 fps for observations of bright sources, thus sources brighter than 30× the *Chandra* pile-up limit can be observed free of pile-up. Faster readout improves time resolution, allows timing studies to take better advantage of the large collecting area; and allows for thinner filters and higher soft X-ray sensitivity. This also dramatically reduces spacecraft requirements on jitter.

3.3 Spacecraft and Mission Operations

The GSFC Mission Design Lab (MDL) studied the *AXIS* mission concept using the instrument (X-ray telescope and detector) point design described above. The estimated instrument mass and power are 751 kg and 297 W, respectively. The total wet mass, including the de-orbit systems, is 2300 kg (including 20% margin). The estimated average and peak *AXIS* power consumption are 720 W and 1200 W, provided by 8.2 m^2 of solar panels producing 2600 W at launch and 1200 W after 10 years of operations. A 145 amp-hour battery provides power during eclipses. The low

*https://ntrs.nasa.gov/search.jsp?R=20170009472

inclination, low-earth orbit minimizes the detector particle background, reduces radiation damage, and allows for rapid communication and response times.

The resulting mission design meets all of the *AXIS* science requirements in a class B mission with a nominal five year lifetime (with consumables sized for at least ten years). The spacecraft meets the mass, length, and diameter specifications for launch into this orbit on a SpaceX Falcon 9.

Optimizing observing efficiency and allowing for rapid response to transients requires a slew rate of 120° in < 6 minutes, accomplished using 6 reaction wheels. Three magnetic torquers dissipate accumulated angular momentum using the Earth's magnetic field. The field of regard is set primarily by requiring a 45° Sun exclusion angle.

Most fields will not require continuous observation to build up the required exposure, enabling a smooth and automatic restart after interruptions caused by ToOs. Despite the large format detectors, the data rate is modest since only X-ray photon events identified by on-board processing are telemetered to the ground. The onboard storage (128 Gbit) and telemetry system were designed to support 4 Gbit/day downlink using two 10-minute S-band ground station passes, and allows for the handling of ground system outages. Data volumes as high as 40 Gbit/day may be accommodated with additional downloads.

Our *AXIS* observations concept will support at least five ToOs per week. The requirement for ToO response, based on the extensive *Swift* legacy, is four hours. Normal operations are designed assuming two downlink passes per day using the Near-Earth Network (NEN), although there are many more opportunities for ToO uplinks. In rare cases, response times as short as one hour are possible by taking advantage of TDRSS. TDRSS would be used during launch and for critical command and control communication.

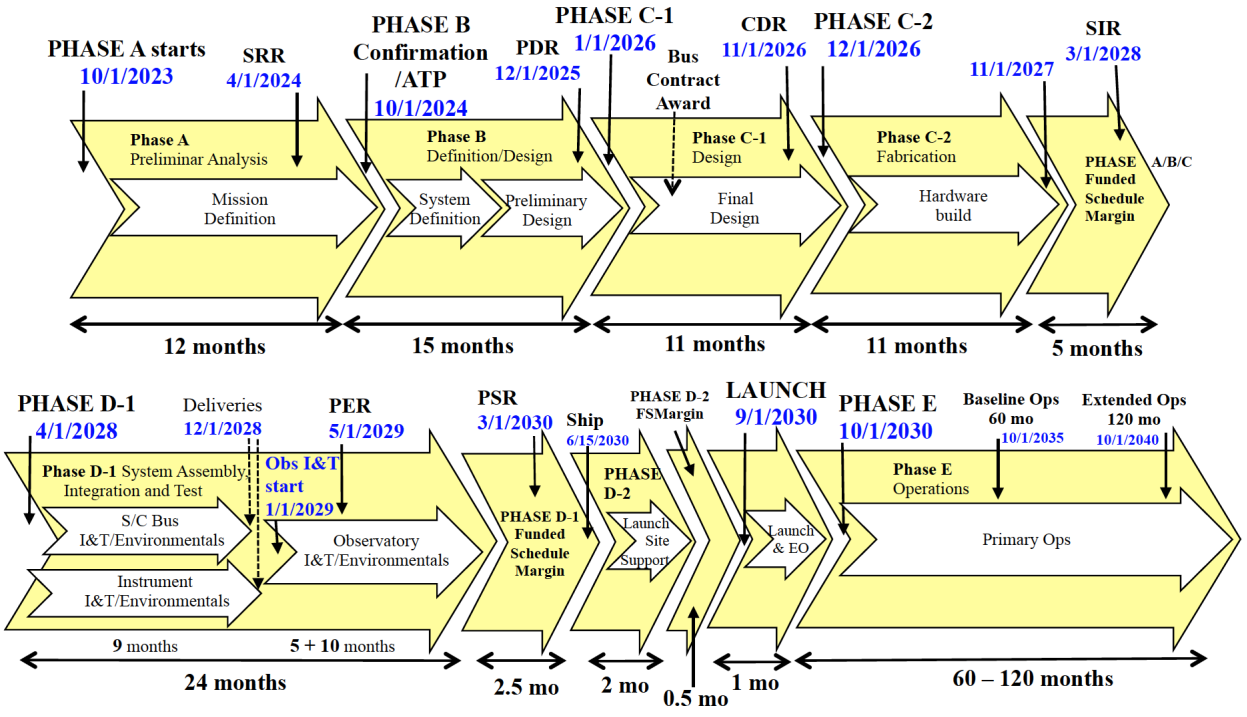

Fig. 9 — The experience-based seven-year *AXIS* mission development schedule (phases A-D).

4 TECHNOLOGY DRIVERS

The most significant technology development necessary is the fabrication of mirror segments and integrating (aligning and bonding) them into mirror modules. The other steps in the mirror fabri-

cation process are routine engineering and I&T work implemented in many past missions.

AXIS's mirror technology is funded at $2.4M/year, a level of funding adequate to achieve TRL-5 by 2022. Additional project-specific funding is needed to achieve TRL-6.

The NGXO team has built and tested a prototype mirror module with a pair of silicon mirrors substantially similar to what AXIS requires, producing an image with 1.2″ HPD at the GSFC beamline. Detailed finite element analysis has shown that, once gravity distortion is accounted for, the underlying quality of the mirror module is 0.5″ HPD, close to meeting AXIS requirements.

5 STATUS, SCHEDULE, AND COST ESTIMATE

The *AXIS* team is a ad hoc group composed of volunteer scientists from a wide variety of institutions. The mission schedule assumed for costing is shown in Figure 9. The *AXIS* launch would occur ∼7 years after the start of Phase-A assuming that TRL 5 is achieved before early 2023.

The *AXIS* mission point design cost (phases A-E, including operations for 5 years) was estimated using standard GSFC Integrated Design Center MDL and IDL methods, applied to a standard work breakdown structure (WBS). The AXIS instrument is defined as a self-contained unit that includes the mirror, detector system and electronics, and the connecting structure (tube). A detailed cost breakdown is included in our full report[1].

Top-level WBS	Source	Cost ($M)
Project Management	Wrap	46
Systems Engineering	Wrap	46
Safety/Mission Assurance	Wrap	29
Mission Science	Wrap	57
Payloads (optics, detector)	IDL/Team	429
Spacecraft	MDL	143
Missions Operations	MDL	54
Launch Vehicle/Services	MDL	150
Ground Systems	Wrap	40
Systems I&T	MDL	17
Total		**$1,012**

Table 2 — A summary of the *AXIS* cost estimate from the GSFC MDL and the *AXIS* team (including 30% reserves).

The costs in Table 2 use a self-developed grassroots tool based on the experience of the last 3 years to refine the mirror cost estimate to $200M, rather than the IDL cost of $60M. We also added $20M to the instrument for a metrology system, not included in the IDL study.

The mission cost estimate (Phases A–E) was generated within the MDL. Reserves of 30% were applied to all WBS elements, except Launch Services (fixed at $150M). The total *AXIS* point design cost estimate, including reserves, is $1,012M. The cost table, which groups some WBS elements, is shown in Table 2.

The limitations of this cost estimate should be noted. In particular, the IDL design represents a point design. While the spacecraft concept is high-heritage and thus presents a low cost growth risk, it contains several known inefficiencies which would be removed through a more thorough design study (e.g., in-house vs. out-of-house, avionics choice, attitude control system, propellant system). Additionally, as documented in the previous X-ray Probes Study[†], the extensive mission operations heritage for *AXIS*-like missions will reduce the operations costs below the wrap value. On the other hand, the cost of some instrument components might be underestimated. Cost growth beyond a putative Probe cost cap can be offset through descopes such that the primary mission science objectives can still be achieved.

[†]https://pcos.gsfc.nasa.gov/studies/completed/x-ray-probe-2013-2014.php

Author	Science White Paper Title
Aalto	Extremely obscured galaxy nuclei, hidden AGNs and extreme starbursts
Basu-Zych	Cooking with X-rays: Can X-ray binaries heat the early Universe?
Blecha	Detecting Offset Active Galactic Nuclei
Bogdanov	Determining the Equation of State of Cold, Dense Matter with X-ray Observations of Neutron Stars
Bulbul	Probing Macro-Scale Gas Motions and Turbulence in Diffuse Cosmic Plasmas
Burns	A Summary of Multimessenger Science with Neutron Star Mergers
Chartas	A New Era for X-ray Lensing Studies of Quasars and Galaxies
Civano	Cosmic evolution of supermassive black holes: A view into the next two decades
Fabbiano	Increasing the Discovery Space in Astrophysics The Exploration Question for Compact Objects
Fan	The First Luminous Quasars and Their Host Galaxies
Gallo	Towards a high accuracy measurement of the local black hole occupation fraction in low mass galaxies
Garcia	Probing the Black Hole Engine with Measurements of the Relativistic X-ray Reflection Component
Gelfand	MeV Emission from Pulsar Wind Nebulae: Understanding Extreme Particle Acceleration in Highly Relativistic Outflows
Hickox	Resolving the cosmic X-ray background with a next-generation high-energy X-ray observatory
Hodges-Kluck	Hot Drivers of Stellar Feedback from 10 to 10,000 pc
Kara	X-ray follow-up of extragalactic transients
Kelley	Multi-Messenger Astrophysics With Pulsar Timing Arrays
Koss	Black Hole Growth in Mergers and Dual AGN
Mantz	The Future Landscape of High-Redshift Galaxy Cluster Science
Markevitch	Physics of cosmic plasmas from high angular resolution X-ray imaging of galaxy clusters
Plotkin	Local Constraints on Supermassive Black Hole Seeds
Reynolds	High-Energy Astrophysics in the 2020s and Beyond
Ruszkowski	Supermassive Black Hole Feedback
Safi-Harb	High-Resolution X-ray Imaging Studies of Neutron Stars, Pulsar Wind Nebulae and Supernova Remnants
Snios	X-rays Studies of the Solar System
Tombesi	Do Supermassive Black Hole Winds Impact Galaxy Evolution?
Valencic	Probing the Structure of Interstellar Dust from Micron to Kpc Scales with X-ray Imaging
Voit	Circumgalactic Gas and the Precipitation Limit
Vulic	Time Domain Studies of Neutron Star and Black Hole Populations: X-ray Identification of Compact Object Types
Walker	Unveiling the Galaxy Cluster - Cosmic Web Connection with X-ray observations in the Next Decade
Williams	Future X-ray Studies of Supernova Remnants
Wolk	X-ray Studies of Exoplanets
Wolk	Understanding Galactic Star Formation with Next-Generation X-ray Spectroscopy and Imaging
Zezas	X-ray binaries: laboratories for understanding the evolution of compact objects from their birth to their mergers

Table 3 — NAS Astro2020 Science White Papers that directly mention *AXIS* by name. Many others would directly benefit from the *AXIS* mission.

6 REFERENCES

1. Mushotzky, R. F. *et al.* The Advanced X-ray Imaging Satellite. *arXiv e-prints* arXiv:1903.04083 (2019).

2. Vito, F. *et al.* The hard X-ray luminosity function of high-redshift ($3 < z \leq 5$) active galactic nuclei. *MNRAS* **445**, 3557–3574 (2014).

3. Vito, F. *et al.* High-redshift AGN in the Chandra Deep Fields: the obscured fraction and space density of the sub-L_* population. *MNRAS* **473**, 2378–2406 (2018).

4. Ricarte, A. & Natarajan, P. The observational signatures of supermassive black hole seeds. *MNRAS* **481**, 3278–3292 (2018).

5. Natarajan, P. *et al.* Unveiling the First Black Holes With JWST:Multi-wavelength Spectral Predictions. *ApJ* **838**, 117 (2017).

6. Pezzulli, E. *et al.* Faint progenitors of luminous $z \sim 6$ quasars: Why do not we see them? *MNRAS* **466**, 2131–2142 (2017).

7. Koss, M. *et al.* Understanding Dual Active Galactic Nucleus Activation in the nearby Universe. *ApJ* **746**, L22 (2012).

8. Steinborn, L. K. *et al.* Origin and properties of dual and offset active galactic nuclei in a cosmological simulation at z=2. *MNRAS* **458**, 1013–1028 (2016).

9. Wang, Q. D. *et al.* Dissecting X-ray-Emitting Gas Around the Center of Our Galaxy. *Science* **341**, 981–983 (2013).

10. Wong, K.-W. *et al.* The Megasecond Chandra X-Ray Visionary Project Observation of NGC 3115: Witnessing the Flow of Hot Gas within the Bondi Radius. *ApJ* **780**, 9 (2014).

11. Russell, H. R. *et al.* The imprints of AGN feedback within a supermassive black hole's sphere of influence. *MNRAS* **477**, 3583–3599 (2018).

12. Paczynski, B. Gravitational microlensing at large optical depth. *ApJ* **301**, 503–516 (1986).

13. Wambsganss, J., Paczynski, B. & Schneider, P. Interpretation of the microlensing event in QSO 2237 + 0305. *ApJ* **358**, L33–L36 (1990).

14. Kochanek, C. S. Quantitative Interpretation of Quasar Microlensing Light Curves. *ApJ* **605**, 58–77 (2004).

15. Chartas, G. *et al.* Measuring the Innermost Stable Circular Orbits of Supermassive Black Holes. *ApJ* **837**, 26 (2017).

16. Pooley, D. *et al.* The Dark-matter Fraction in the Elliptical Galaxy Lensing the Quasar PG 1115+080. *ApJ* **697**, 1892–1900 (2009).

17. Chartas, G. *et al.* Gravitational lensing size scales for quasars. *Astronomische Nachrichten* **337**, 356 (2016).

18. Dai, X., Steele, S., Guerras, E., Morgan, C. W. & Chen, B. Constraining Quasar Relativistic Reflection Regions and Spins with Microlensing. *ApJ* **879**, 35 (2019).

19. Rees, M. J. Tidal disruption of stars by black holes of 10 to the 6th-10 to the 8th solar masses in nearby galaxies. *Nature* **333**, 523–528 (1988).

20. Coughlin, E. R. & Begelman, M. C. Hyperaccretion during Tidal Disruption Events: Weakly Bound Debris Envelopes and Jets. *ApJ* **781**, 82 (2014).

21. Lin, D. *et al.* A luminous X-ray outburst from an intermediate-mass black hole in an off-centre star cluster. *Nature Astronomy* **2**, 656–661 (2018).

22. Troja, E. *et al.* The outflow structure of GW170817 from late-time broad-band observations. *MNRAS* **478**, L18–L23 (2018).

23. Dal Canton, T. *et al.* Detectability of modulated X-rays from LISA's supermassive black hole mergers. *arXiv e-prints* arXiv:1902.01538 (2019).

24. Bachetti, M. *et al.* An ultraluminous X-ray source powered by an accreting neutron star. *Nature* **514**, 202–204 (2014).

25. Dolag, K., Meneghetti, M., Moscardini, L., Rasia, E. & Bonaldi, A. Simulating the physical properties of dark matter and gas inside the cosmic web. *MNRAS* **370**, 656–672 (2006).

26. Lehmer, B. D. *et al.* A Chandra Perspective on Galaxy-wide X-ray Binary Emission and its Correlation with Star Formation Rate and Stellar Mass: New Results from Luminous Infrared Galaxies. *ApJ* **724**, 559–571 (2010).

27. Lehmer, B. D. *et al.* The Evolution of Normal Galaxy X-Ray Emission through Cosmic History: Constraints from the 6 MS Chandra Deep Field-South. *ApJ* **825**, 7 (2016).

28. Negrello, M. *et al.* The Herschel-ATLAS: a sample of 500 μm-selected lensed galaxies over 600 deg^2. *MNRAS* **465**, 3558–3580 (2017).

29. Dye, S. *et al.* Revealing the complex nature of the strong gravitationally lensed system H-ATLAS J090311.6+003906 using ALMA. *MNRAS* **452**, 2258–2268 (2015).

30. White, S. D. M. & Frenk, C. S. Galaxy formation through hierarchical clustering. *ApJ* **379**, 52–79 (1991).

31. Walker, S. *et al.* The Physics of Galaxy Cluster Outskirts. *Space Sci. Rev.* **215**, 7 (2019).

32. Bregman, J. N. *et al.* The Extended Distribution of Baryons around Galaxies. *ApJ* **862**, 3 (2018).

33. Power, C. *et al.* nIFTy Galaxy Cluster simulations VI: The gaseous outskirts of galaxy cluster. *arXiv e-prints* (2018).

34. Sanders, J. S., Fabian, A. C., Russell, H. R., Walker, S. A. & Blundell, K. M. Detecting edges in the X-ray surface brightness of galaxy clusters. *MNRAS* **460**, 1898–1911 (2016).

35. Babyk, I. V. *et al.* A Universal Entropy Profile for the Hot Atmospheres of Galaxies and Clusters within R $_{2500}$. *ApJ* **862**, 39 (2018).

36. Faucher-Giguère, C.-A. & Quataert, E. The physics of galactic winds driven by active galactic nuclei. *MNRAS* **425**, 605–622 (2012).

37. Veilleux, S., Cecil, G. & Bland-Hawthorn, J. Galactic Winds. *ARA&A* **43**, 769–826 (2005).

38. Heckman, T. M. & Thompson, T. A. A Brief Review of Galactic Winds. *arXiv e-prints* (2017).

39. Heckman, T. M. *et al.* The Properties of Ultraviolet-luminous Galaxies at the Current Epoch. *ApJ* **619**, L35–L38 (2005).

40. Cardamone, C. *et al.* Galaxy Zoo Green Peas: discovery of a class of compact extremely star-forming galaxies. *MNRAS* **399**, 1191–1205 (2009).

41. Izotov, Y. I. *et al.* Eight per cent leakage of Lyman continuum photons from a compact, star-forming dwarf galaxy. *Nature* **529**, 178–180 (2016).

42. Zeldovich, Y. B. & Raizer, Y. P. *Elements of gasdynamics and the classical theory of shock waves* (Academic Press, New York, NY, ed. W.D. Hayes & R.F. Probstein, 1966).

43. Markevitch, M. Chandra Observation of the Most Interesting Cluster in the Universe. In Wilson, A. (ed.) *The X-ray Universe 2005*, vol. 604 of *ESA Special Publication*, 723 (2006). astro-ph/0511345.

44. Russell, H. R. *et al.* Shock fronts, electron-ion equilibration and intracluster medium transport processes in the merging cluster Abell 2146. *MNRAS* **423**, 236–255 (2012).

45. Wang, Q. H. S., Giacintucci, S. & Markevitch, M. Bow Shock in Merging Cluster A520: The Edge of the Radio Halo and the Electron-Proton Equilibration Timescale. *ApJ* **856**, 162 (2018).

46. Markevitch, M. & Vikhlinin, A. Shocks and cold fronts in galaxy clusters. *Phys. Rep.* **443**, 1–53 (2007).

47. Ascasibar, Y. & Markevitch, M. The Origin of Cold Fronts in the Cores of Relaxed Galaxy Clusters. *ApJ* **650**, 102–127 (2006).

48. Roediger, E. *et al.* Viscous Kelvin-Helmholtz instabilities in highly ionized plasmas. *MNRAS* **436**, 1721–1740 (2013).

49. ZuHone, J. A., Kunz, M. W., Markevitch, M., Stone, J. M. & Biffi, V. The Effect of Anisotropic Viscosity on Cold Fronts in Galaxy Clusters. *ApJ* **798**, 90 (2015).

50. Roediger, E., Kraft, R. P., Forman, W. R., Nulsen, P. E. J. & Churazov, E. Kelvin-Helmholtz Instabilities at the Sloshing Cold Fronts in the Virgo Cluster as a Measure for the Effective Intracluster Medium Viscosity. *ApJ* **764**, 60 (2013).

51. Su, Y. *et al.* Deep Chandra Observations of NGC 1404: Cluster Plasma Physics Revealed by an Infalling Early-type Galaxy. *ApJ* **834**, 74 (2017).

52. Ichinohe, Y., Simionescu, A., Werner, N. & Takahashi, T. An azimuthally resolved study of the cold front in Abell 3667. *MNRAS* **467**, 3662–3676 (2017).

53. Wang, Q. H. S. & Markevitch, M. A Deep X-Ray Look at Abell 2142 – Viscosity Constraints From Kelvin-Helmholtz Eddies, a Displaced Cool Peak That Makes a Warm Core, and A Possible Plasma Depletion Layer. *ApJ* **868**, 45 (2018).

54. Tran, A., Williams, B. J., Petre, R., Ressler, S. M. & Reynolds, S. P. Energy Dependence of Synchrotron X-Ray Rims in Tycho's Supernova Remnant. *ApJ* **812**, 101 (2015).

55. Ressler, S. M. *et al.* Magnetic Field Amplification in the Thin X-Ray Rims of SN 1006. *ApJ* **790**, 85 (2014).

56. Winkler, P. F. *et al.* A High-resolution X-Ray and Optical Study of SN 1006: Asymmetric Expansion and Small-scale Structure in a Type Ia Supernova Remnant. *ApJ* **781**, 65 (2014).

57. Zhang, W. W. & et al. High-resolution, Lightweight, and Low-cost X-ray Optics for the Lynx Observatory. *J. of Astronomical Telescopes, Instruments, and Systems* **5**, 021012 (2019).

58. Bautz, M. *et al.* Toward fast low-noise low-power digital CCDs for Lynx and other high-energy astrophysics missions. In *Space Telescopes and Instrumentation 2018: Ultraviolet to Gamma Ray*, vol. 10699 of *Society of Photo-Optical Instrumentation Engineers (SPIE) Conference Series*, 1069917 (2018).

59. Li, J. *et al.* Chandra ACIS Subpixel Event Repositioning: Further Refinements and Comparison between Backside- and Frontside-illuminated X-Ray CCDs. *ApJ* **610**, 1204–1212 (2004).

60. Bray, E., Burrows, D. N., Falcone, A. D., Wages, M. & Chattopadhyay, T. Exploring fine subpixel spatial resolution of hybrid CMOS detectors. In *Space Telescopes and Instrumentation 2018: Ultraviolet to Gamma Ray*, no. 10699204 in Proc. SPIE (2018).

61. Miller, E. D. *et al.* The effects of charge diffusion on soft x-ray response for future high-resolution imagers. In *Society of Photo-Optical Instrumentation Engineers (SPIE) Conference Series*, vol. 10699 of *Society of Photo-Optical Instrumentation Engineers (SPIE) Conference Series*, 106995R (2018).